**Supplemental information**

Nutrient-sensing AgRP neurons relay control
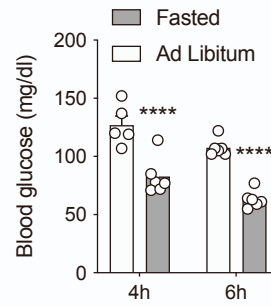
# of liver autophagy during energy deprivation

Weiyi Chen, Oliver Mehlkop, Alexandra Scharn, Hendrik Nolte, Paul Klemm, Sinika Henschke, Lukas Steuernagel, Tamara Sotelo-Hitschfeld, Ecem Kaya, Claudia Maria Wunderlich, Thomas Langer, Natalia L. Kononenko, Patrick Giavalisco, and Jens Claus Brüning
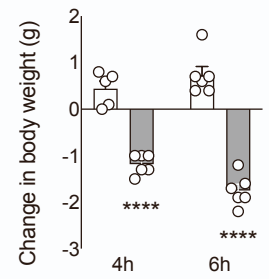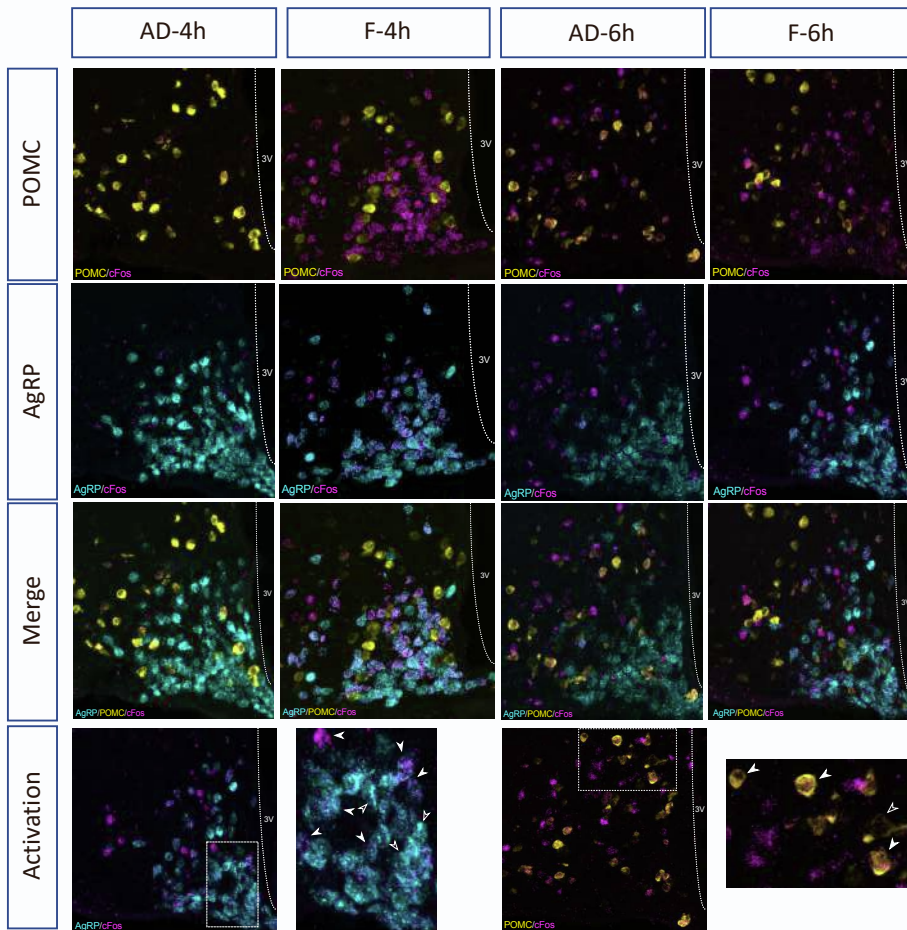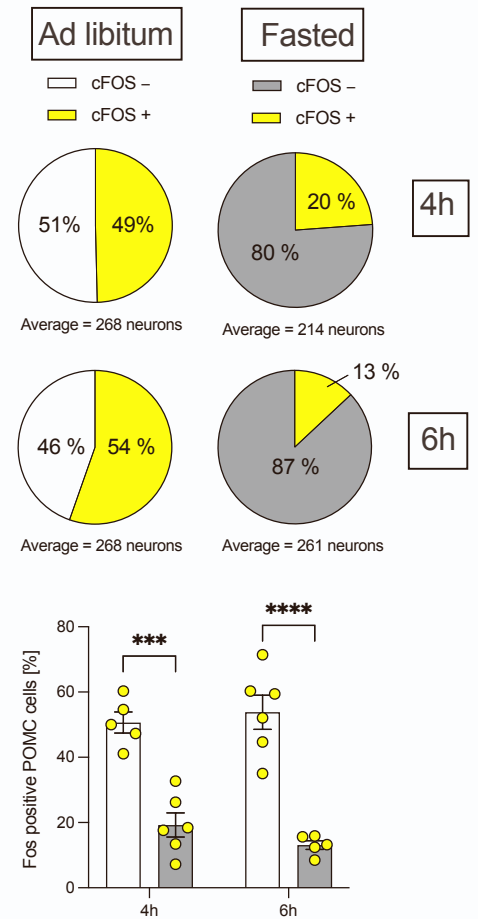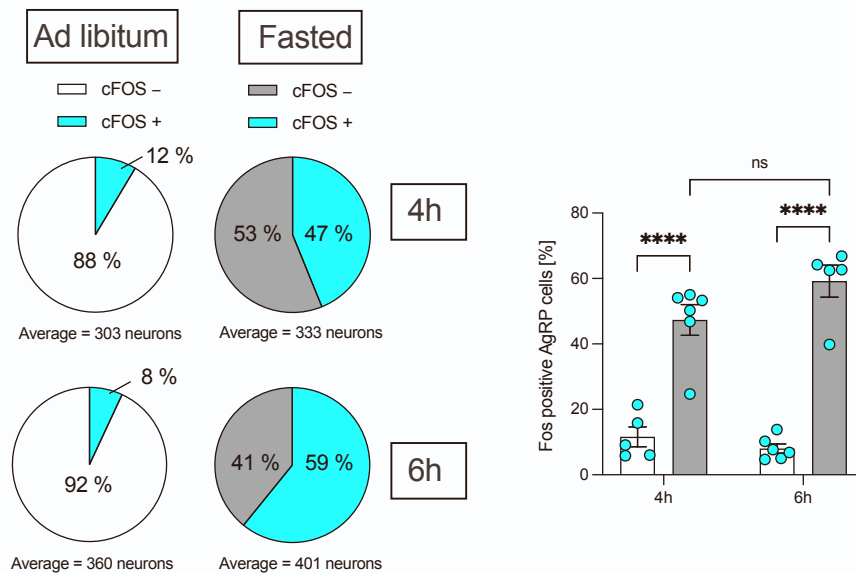
Supplemental Figure 1
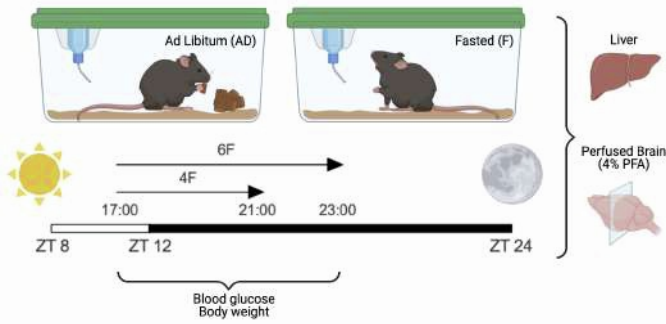
Figure S1. Short-term fasting activates AgRP neurons and inhibits POMC neurons, related to Figure 1.

(A)   Experimental design for short-term fasting of C57Bl/6N mice.

(B)   Blood glucose concentrations of ad libitum fed and fasted C57Bl/6N mice at ZT15 and ZT17 respectively (n = 5-6 animals/group/timepoint).

(C)   Change in body weight after 4 h and 6 h of fasting into the dark cycle (n = 5-6 animals/group/timepoint).
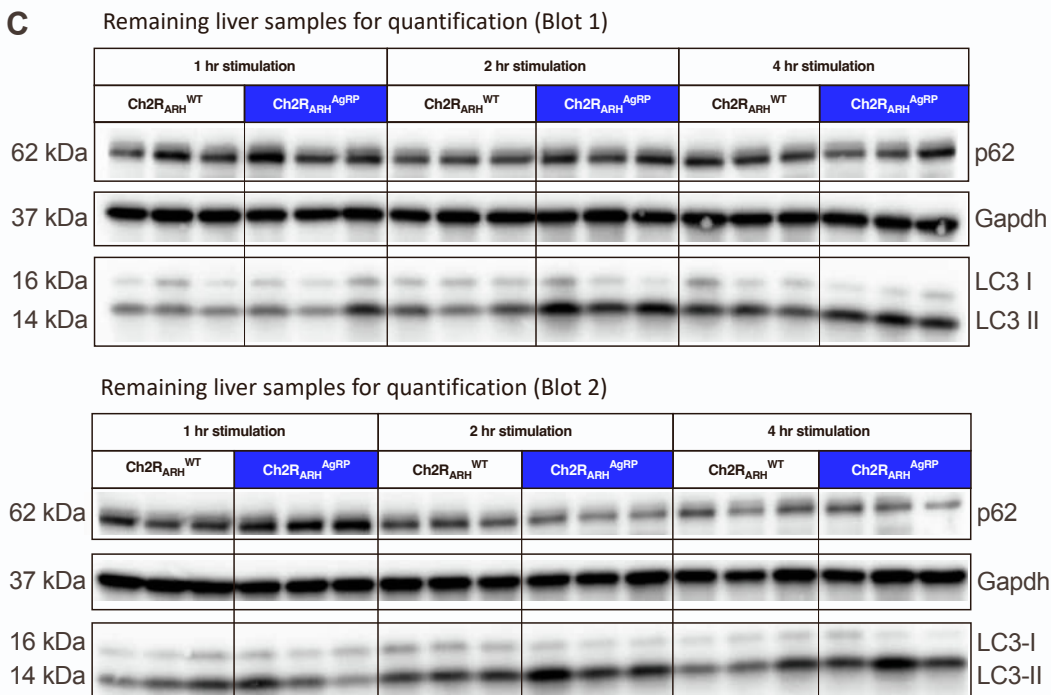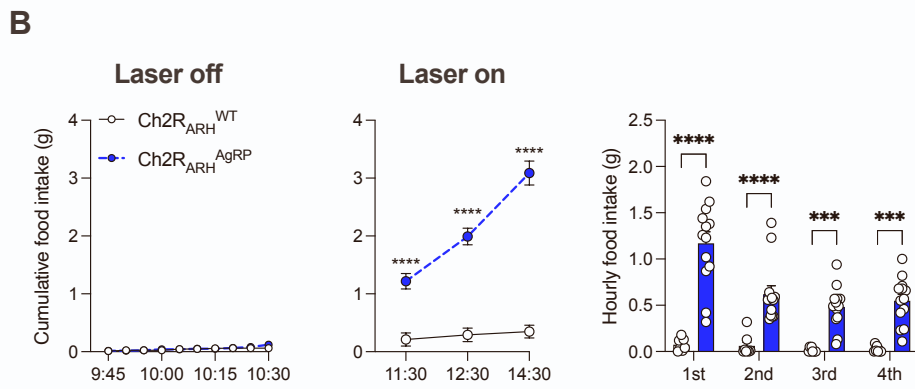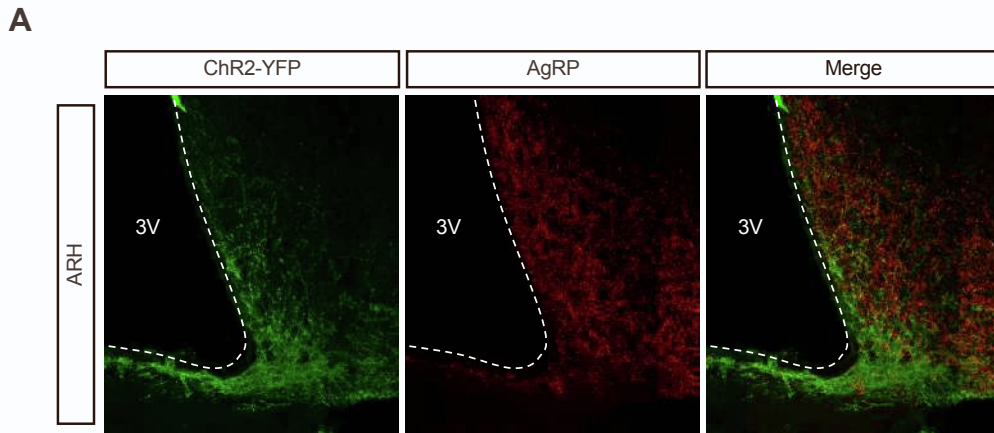
(D)   Representative confocal images showing *AgRP* (Cyan), *POMC* (Yellow) and *cFos* (Magenta) mRNA expression in the ARH of ad libitum fed (AD) or fasted (F) mice for 4 h and 6 h into the dark cycle respectively. Bottom panel depicts activated AgRP and POMC neuron as indicated by white arrows.

(E)   Quantification of *cFos* positive POMC cells in the ARH using mRNA *in situ* hybridization. Results presented as individual datapoints, indicating the percentage of *Fos* positive cells over POMC cells counted (n = 5-6 animals/group/timepoint).

(F)   Quantification of *cFos* positive AgRP cells in the ARH using mRNA *in situ* hybridization. Results presented as individual datapoints, indicating the percentage of *Fos* positive AgRP (n = 5-6 animals/group/timepoint).

Data are represented as mean ± SEM. Statistical analyses were performed by two-way ANOVA followed by Šídák post hoc test. ns = not significant, ***$p \leq 0.001$, ****$p \leq 0.0001$.

Supplemental Figure 2

A

B

C

Remaining liver samples for quantification (Blot 1)

Remaining liver samples for quantification (Blot 2)

Figure S2. Time-dependent induction of autophagic flux upon AgRP neuron activation, related to Figure 1.

(A)   Immunofluorescent staining validating ChR2 expression (ChR2-EYFP-IR, Green) and AgRP fibers (AgRP-IR, Red) and the co-localization in the ARH (Merge).
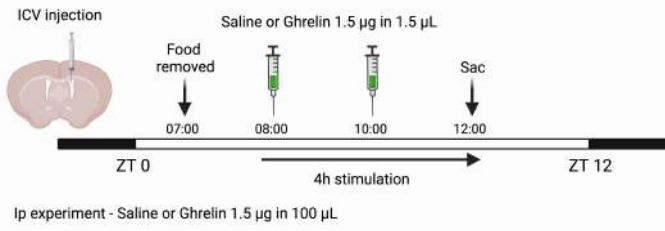
(B)   Pre-laser, cumulative and hourly food intake measurements following AgRP neuron photostimulation (n = 5-13 animals/group).

(C)   Western blots of hepatic expression of autophagic markers (LC3 and p62) for individual mice after 1 h, 2 h and 4 h photostimulation of AgRP neurons.
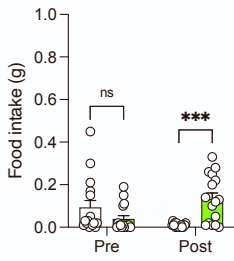
Data are represented as mean ± SEM. Statistical analyses were performed by two-way ANOVA with RM for treatment followed by Šídák post hoc test.
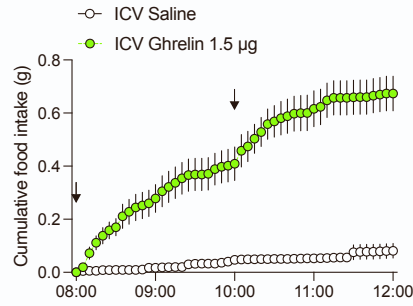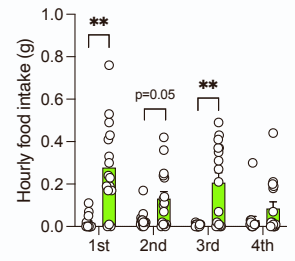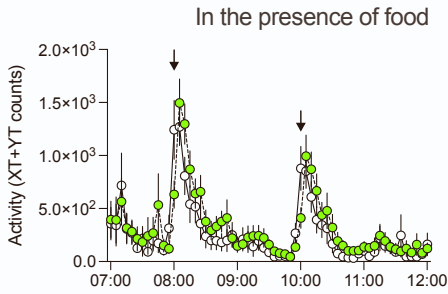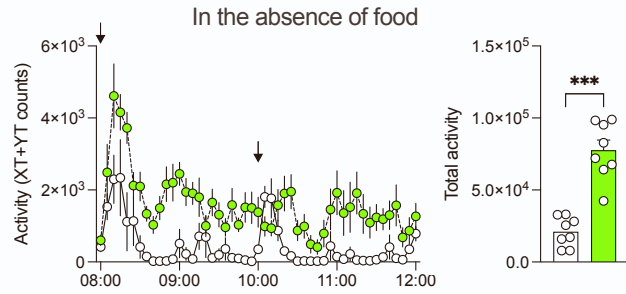
Supplemental Figure 3

A

ICV injection

Food removed — Saline or Ghrelin 1.5 µg in 1.5 µL — Sac

07:00   08:00   10:00   12:00

ZT 0   ZT 12

4h stimulation

Ip experiment - Saline or Ghrelin 1.5 µg in 100 µL

B

Food intake (g)

Pre — ns

Post — ***

C

○ ICV Saline
● ICV Ghrelin 1.5 µg

Cumulative food intake (g)

08:00 09:00 10:00 11:00 12:00

1h *** 2h *** 4h ****

D

Hourly food intake (g)

1st ** 2nd p=0.05 3rd ** 4th

E

In the presence of food

Activity (XT+YT counts)

07:00 08:00 09:00 10:00 11:00 12:00

F

In the absence of food

Activity (XT+YT counts)

08:00 09:00 10:00 11:00 12:00

Total activity ***

G

	AgRP	GhSR	cFOS	Merged
ICV - Saline				
ICV - Ghrelin				

H

Fos positive cells expressing AgRP and GhSR [%]

Saline   Ghrelin   ****

Saline
9.25% cFos +
90.75% cFos -
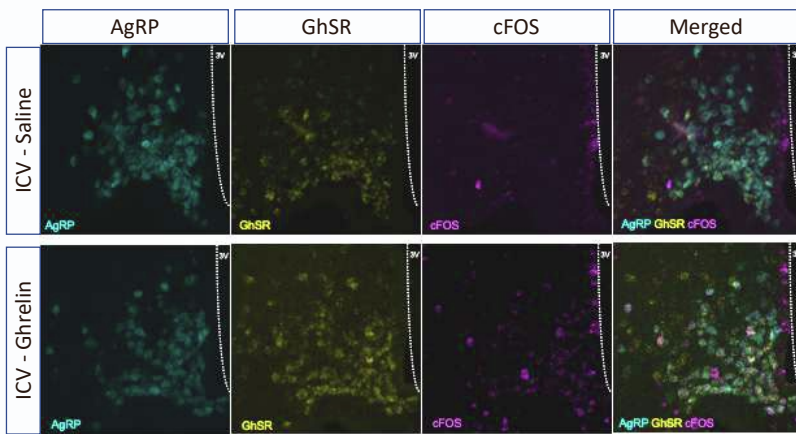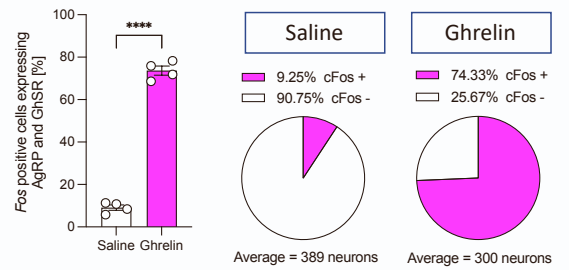Average = 389 neurons

Ghrelin
74.33% cFos +
25.67% cFos -
Average = 300 neurons

Figure S3. Central ghrelin evokes feeding through AgRP neurons, related to Figure 1.

(A)   Workflow and experimental design for the ip and icv administration of ghrelin in C57Bl/6N mice.

(B)   Total food intake over a period of 1 h pre and post icv delivery of either saline or ghrelin in C57Bl/6N mice (n = 16 animals/group; crossover experiment).

(C)   Cumulative food intake over a period of 4 h following either icv saline or Ghrelin injection as indicated by the black arrows. (Right) Depiction of cumulative food intake after 1 h, 2 h and 4 h of central ghrelin action (n = 16 animals/group; crossover experiment).

(D)   Hourly food intake measurements following either icv saline or Ghrelin injection (n = 16 animals/group; crossover experiment).

(E)   Activity recorded over a period of 4 h after either icv saline or Ghrelin injection in the presence of food. Black arrows indicate the injection timepoints (n = 16 animals/group; crossover experiment).

(F)   Activity recorded over a period of 4 h after either icv saline or Ghrelin injection in the absence of food. (Right) Total activity is represented as scatter dot plots with individual values compared to saline group. Black arrows indicate the injection timepoints (n = 8 animals/group).

(G)   Representative confocal images showing *AgRP* (Cyan), *GhSR* (Yellow) and *cFos* (Magenta) mRNA expression in the ARH of C57Bl/6N mice icv injected with either saline or Ghrelin.

(H)   Quantification of *Fos* positive GhSR-expressing AgRP neurons in the ARH of C57Bl/6N mice with either icv saline or Ghrelin using *in situ* hybridization of mRNA (n = 4 animals for quantification). Results are presented as individual datapoints, indicating the percentage of *Fos* positive cells over total colocalizing AgRP and GhSR cells counted.
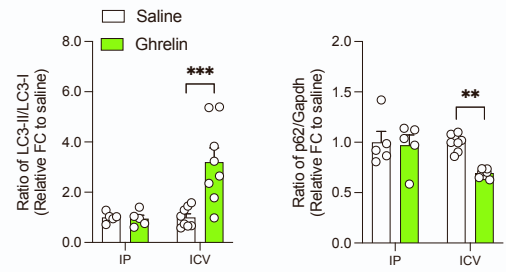
Data are represented as mean ± SEM. Statistical analyses were performed by two-way ANOVA followed by Šídák post hoc test (for B, C and D; RM for treatment) or unpaired two-tailed Student's t test (for F; total activity and H). ns = not significant, **$p \leq 0.01$, ***$p \leq 0.001$, ****$p \leq 0.0001$.
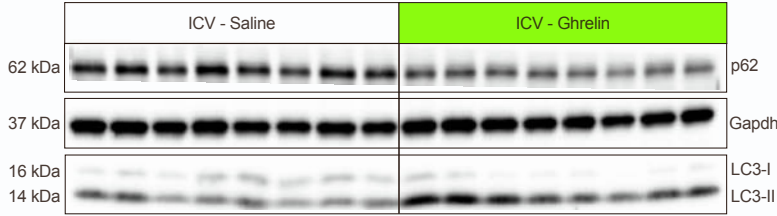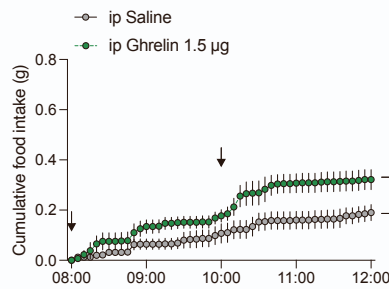
Supplemental Figure 4
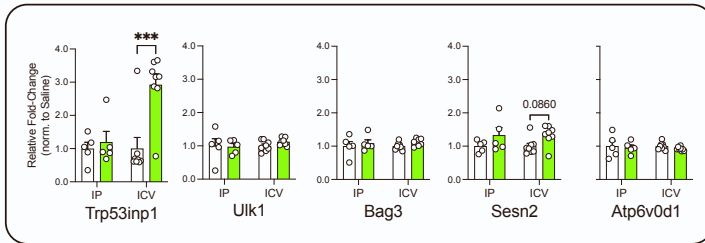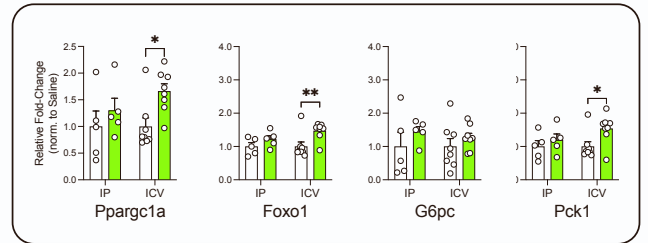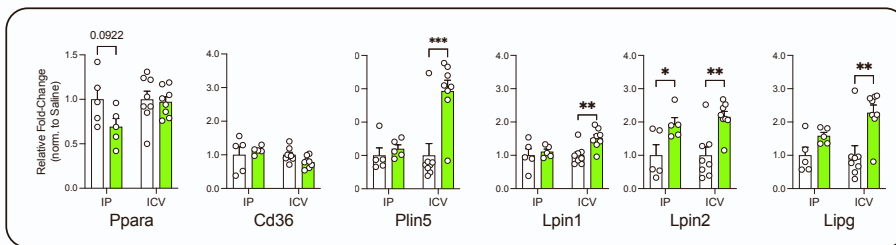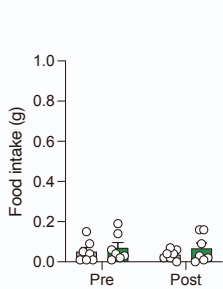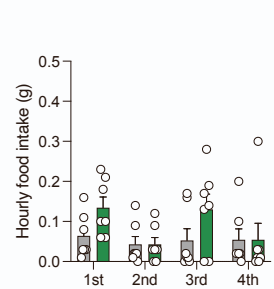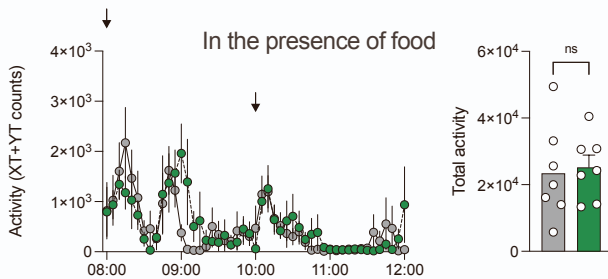
Figure S4. Central Ghrelin action on AgRP neuron promotes hepatic autophagy, related to Figure 1 and S3.

(A)   Representative Western blots of liver homogenates from C57Bl6/N mice which received ip saline, ip Ghrelin, icv saline or icv Ghrelin. Gapdh was used as a loading control.

(B)   Densitometric analysis of the autophagic marker proteins in post-nuclear supernatants of liver homogenates of C57Bl6/N mice which received ip saline or Ghrelin (n = 5 animals/group) and icv saline or Ghrelin (n = 8 animals/group).

(C)   Western blots of hepatic expression of autophagic markers (LC3 and p62) for individual mice after icv injection of saline or Ghrelin.

(D)   Western blots of hepatic expression of autophagic markers (LC3 and p62) for individual mice after ip injection of saline or ghrelin.

(E)   Quantitative real-time PCR analyses of genes related to autophagy, glucose, lipid metabolism and fatty acid oxidation; data are normalized to the respective control group and represented as scatter dot plots with individual values relative to *Tbp* expression (n = 5-8 animals/group).

(F)   Total food intake over a period of 1 h pre and post ip delivery of either saline or ghrelin in C57Bl/6N mice (n = 7 animals/group; crossover experiment).

(G)   Cumulative food intake over a period of 4 h following either ip saline or Ghrelin injection as indicated by the black arrows. (Right) Depiction of cumulative food intake after 1 h, 2 h and 4 h of peripheral ghrelin action (n = 7 animals/group; crossover experiment).

(H)   Hourly food intake measurements following either ip saline or Ghrelin injection (n = 7 animals/ group; crossover experiment).

(I)   Activity recorded over a period of 4 h after either ip saline or Ghrelin injection in the presence of food. Black arrows indicate injection timepoints (n = 7 animals/group; crossover experiment).

Data are represented as mean ± SEM. Statistical analyses were performed by RM two-way ANOVA followed by Šídák post hoc test (for B and E; without RM for treatment, F, G and H; RM for treatment) or unpaired two-tailed Student's t test (for I; Total activity). ns = not significant, *$p \leq 0.05$, **$p \leq 0.01$, ***$p \leq 0.001$.

Supplemental Figure 5

A

B

C

D

E

Autophagy

Glucose metabolism

Lipid metabolism
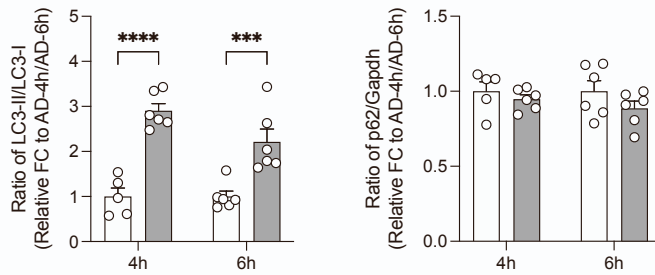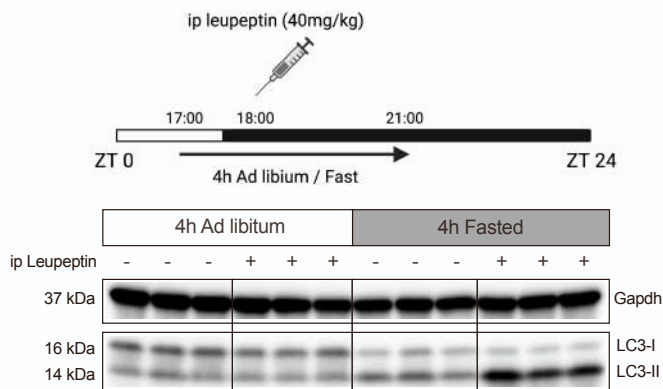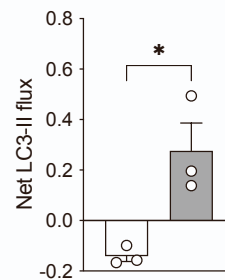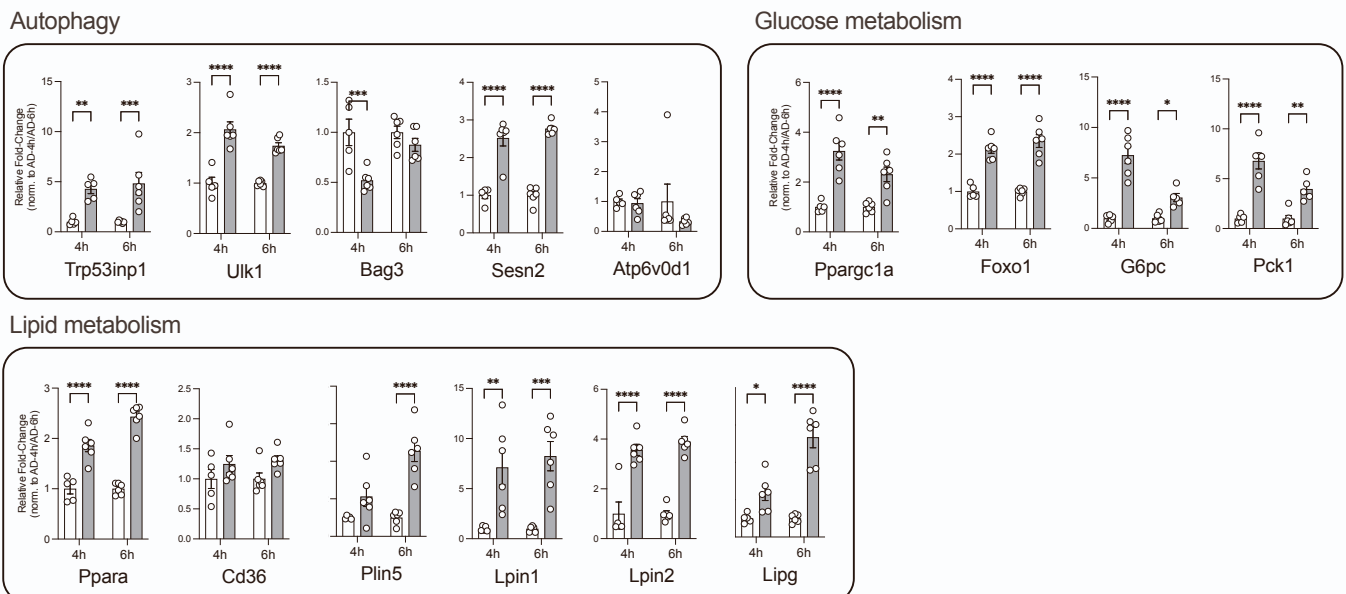
Figure S5. Short-term fasting induces autophagy flux in the liver, related to Figure 1 and S1.

(A)   Representative Western blots of liver extracts from ad libitum fed (AD) or fasted (F) C57Bl6/N mice for 4 h and 6 h into the dark cycle respectively. Gapdh served as loading control.

(B)   Densitometric analysis of the ratio of LC3-II/LC3-I (LC3) and p62/Gapdh as autophagic marker proteins in liver homogenates from mice in (A) (n = 5-6 animals/group).

(C)   Experimental design and representative Western blot analysis of liver homogenates from leupeptin-based LC3-II flux analysis *in vivo* following a short-term fasting paradigm during the feeding cycle. Mice were injected with saline as controls (n = 3 animals/group).
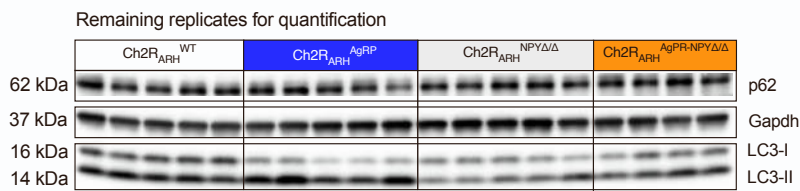
(D)   Net LC3-II flux in the liver as described in (C) (n = 3 animals/group).

(E)   Quantitative real-time PCR analyses of genes related to autophagy, glucose, lipid metabolism and fatty acid oxidation; data are normalized to the respective AD-4h or AD-6h group and represented as scatter dot plots with individual values relative to *Tbp* expression (n =5-6 animals/ group/timepoint)
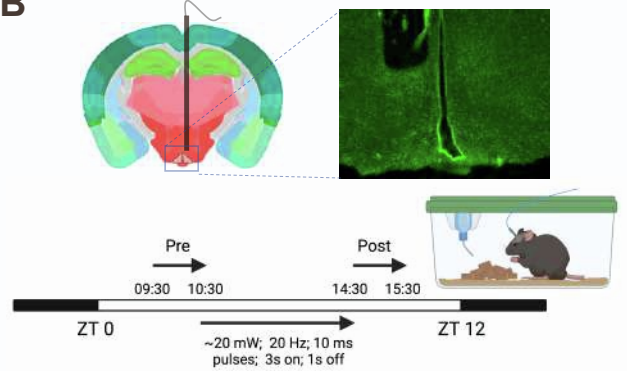
Data are represented as mean ± SEM. Statistical analyses were performed by two-way ANOVA followed by Šídák post hoc test (for B and E) or unpaired two-tailed Student's t test (for D). *$p \leq 0.05$; **$p \leq 0.01$; ***$p \leq 0.001$, ****$p \leq 0.0001$.
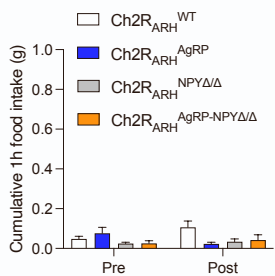
Supplemental Figure 6

A

B
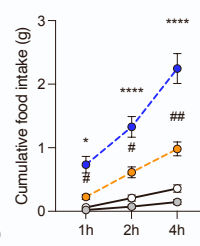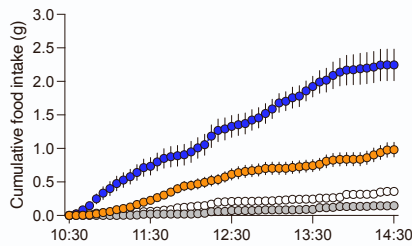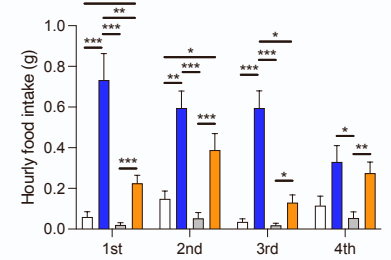

C

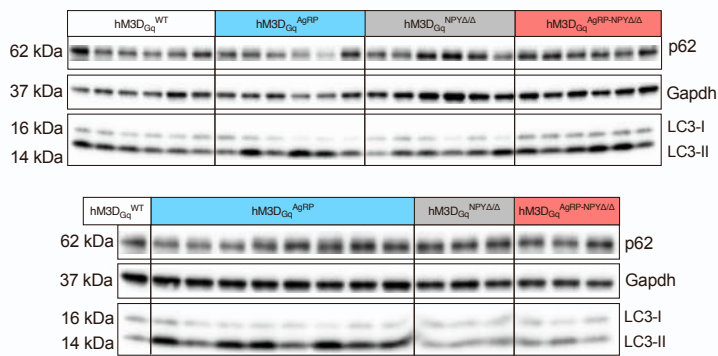
D

E

F

G

Remaining replicates for quantification

H

Autophagy

Glucose metabolism

Lipid Metabolism

AAV-DIO-mCherry
or
AAV-DIO-NPY

Intra-ARH injection and
photostimulation
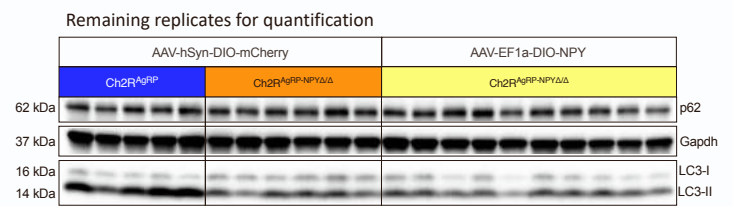
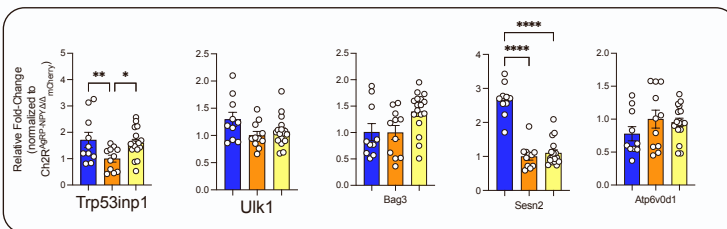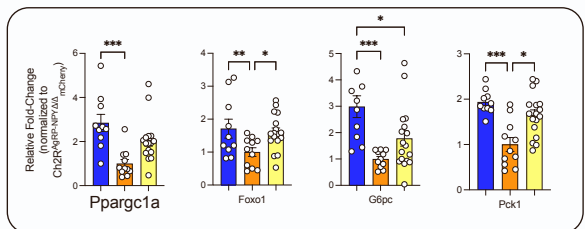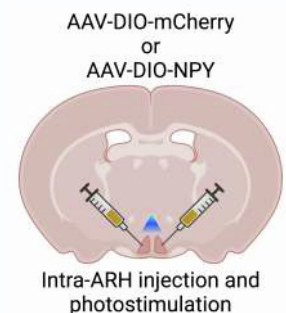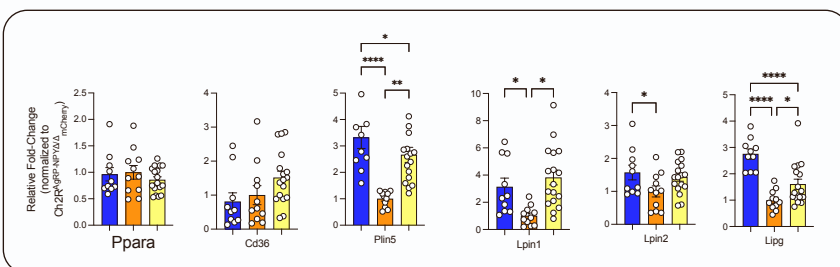**Figure S6. AgRP-mediated control of hepatic autophagy is dependent on NPY expression, related to Figure 2.**

(A)   Western blot showing the remaining replicates for the quantification of hepatic autophagic markers (LC3 and p62) after 4 h optogenetic stimulation of AgRP neuron in the presence and absence of NPY, related to Figures 2B, C.

(B)   Experimental timeline for optogenetic stimulation and verification of optical fiber placement.

(C)   Total food intake over a period of 1 h before light illumination (pre) and 1 h after the lasers were switched off (post) in $ChR2^{WT}$, $ChR2^{AgRP}$, $ChR2^{NPY/}$ and $ChR2^{AgRP-NPY/}$ mice (n = 14-21 animals/genotype).

(D)   Cumulative food intake over a period of 4 h in 5 min intervals. Cumulative food intake after 1 h, 2 h and 4 h of light illumination (n = 14-21 animals/genotype).

(E)   Hourly food intake measurements.

(F)   Western blots showing hepatic protein levels of autophagic markers (LC3 and p62) of individual animals after CNO-mediated activation of AgRP neuron in the presence and absence of NPY, related to Figure 2F, G.
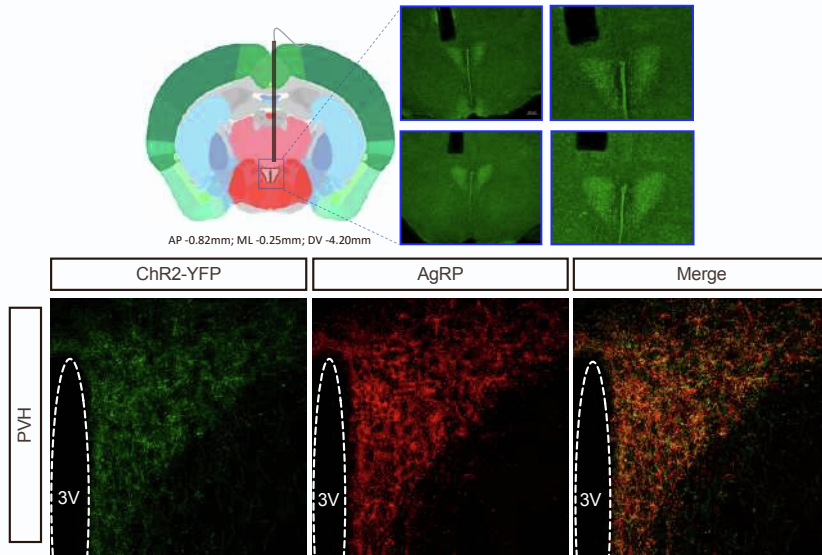
(G)   Western blots showing the remaining replicates of hepatic protein levels of autophagic markers (LC3 and p62) for the re-expression of NPY specifically in AgRP neuron following 4 h of photostimulation, related to Figure 2I, J.

(H)   Quantitative real-time PCR analyses of genes related to autophagy, glucose, lipid metabolism and fatty acid oxidation; data are normalized to $ChR2^{AgRP-NPY/}$ group injected with AAV-DIO-mCherry and represented as scatter dot plots with individual values relative to *Tbp* expression (n =10-11 animals/group)
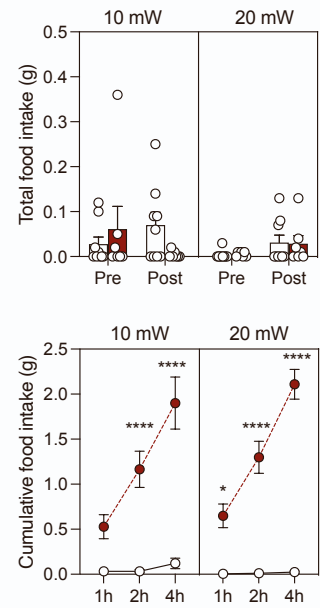
Data are represented as mean ± SEM. Statistical analyses were performed by two-way ANOVA followed by Šídák post hoc test (for C, D and E) or one-way ANOVA followed by Tukey's post hoc test (for H). $*p \leq 0.05$; $**p \leq 0.01$; $***p \leq 0.001$, $****p \leq 0.0001$ vs $ChR2^{WT}$ or $ChR2^{AgRP-NPY/}$, $^{\#}p \leq 0.05$; $^{\#\#}p \leq 0.01$ vs $ChR2^{AgRP}$)

Supplemental Figure 7

A

AP -0.82mm; ML -0.25mm; DV -4.20mm

B

C

AP -1.60m; ML ±1.05mm; DV -4.55mm

D

E

AP -0.45mm; ML ±0.5mm; DV -3.8mm

F

Figure S7. AgRP terminal stimulation promotes feeding, related to Figure 3.

(A)   Micrographs of optical fiber placement and immunofluorescent staining validating ChR2 expression (ChR2-EYFP-IR, Green), immunoreactive AgRP fibers (AgRP-IR, Red) and their co-localization in the PVH (Orange).

(B)   Total food intake 1 h pre and post light illumination. Cumulative food intake over a period of 4 h following 10 mW and 20 mW of light illumination in the PVH (n = 7-9 animals/genotype).

(C)   Micrographs of optical fiber placement and immunofluorescent staining validating ChR2 expression (ChR2-EYFP-IR, Green), immunoreactive AgRP fibers (AgRP-IR, Red) and their co-localization in the LHA (Orange).

(D)   Total food intake 1 h pre and post light illumination. Cumulative food intake over a period of 4 h following 10 mW and 20 mW of light illumination in the LHA (n = 8 animals/genotype).

(E)   Micrographs of optical fiber placement and immunofluorescent staining validating ChR2 expression (ChR2-EYFP-IR, Green), immunoreactive AgRP fibers (AgRP-IR, Red) and their co-localization in the BNST (Orange).

(F)   Total food intake 1 h pre and post light illumination. Cumulative food intake over a period of 4 h following 10 mW and 20 mW of light illumination in the BNST (n = 7 animals/genotype).

Data are represented as mean ± SEM. Statistical analyses were performed by three-way ANOVA followed by Tukey's post hoc test (for B, D and F, RM for laser power and timepoint). *$p \leq 0.05$; ***$p \leq 0.001$, ****$p \leq 0.0001$ vs $ChR2_{PVH}^{WT}$ or $ChR2_{LHA}^{WT}$ or $ChR2_{BNST}^{WT}$)
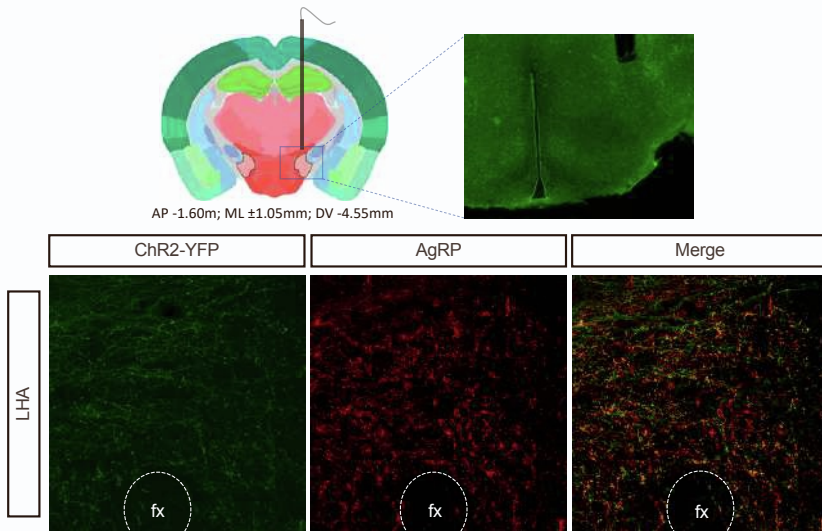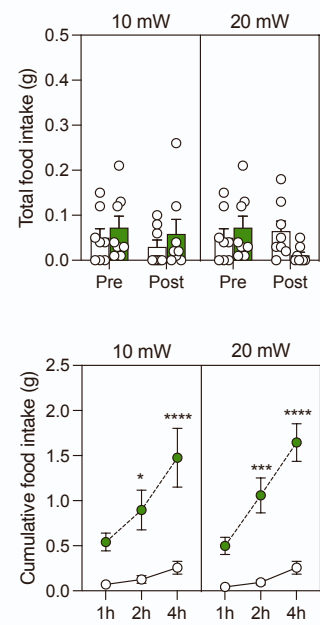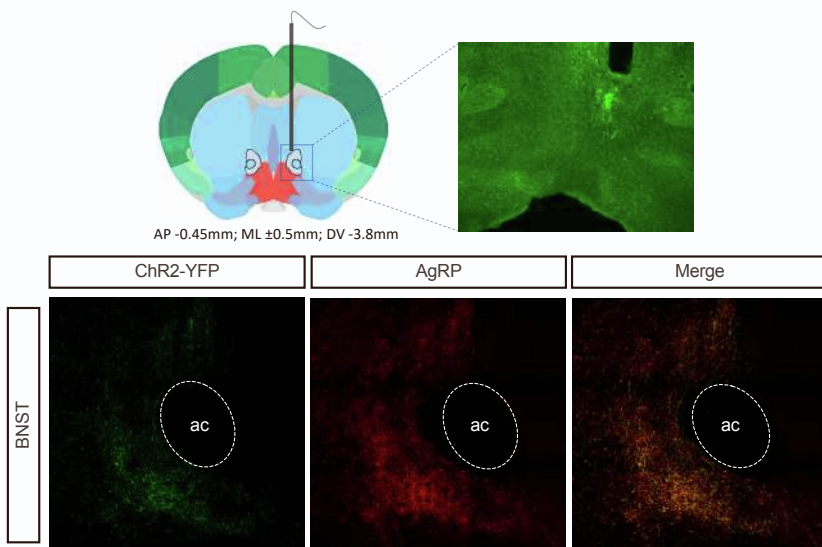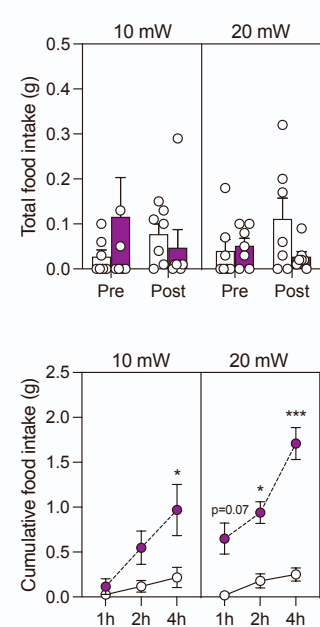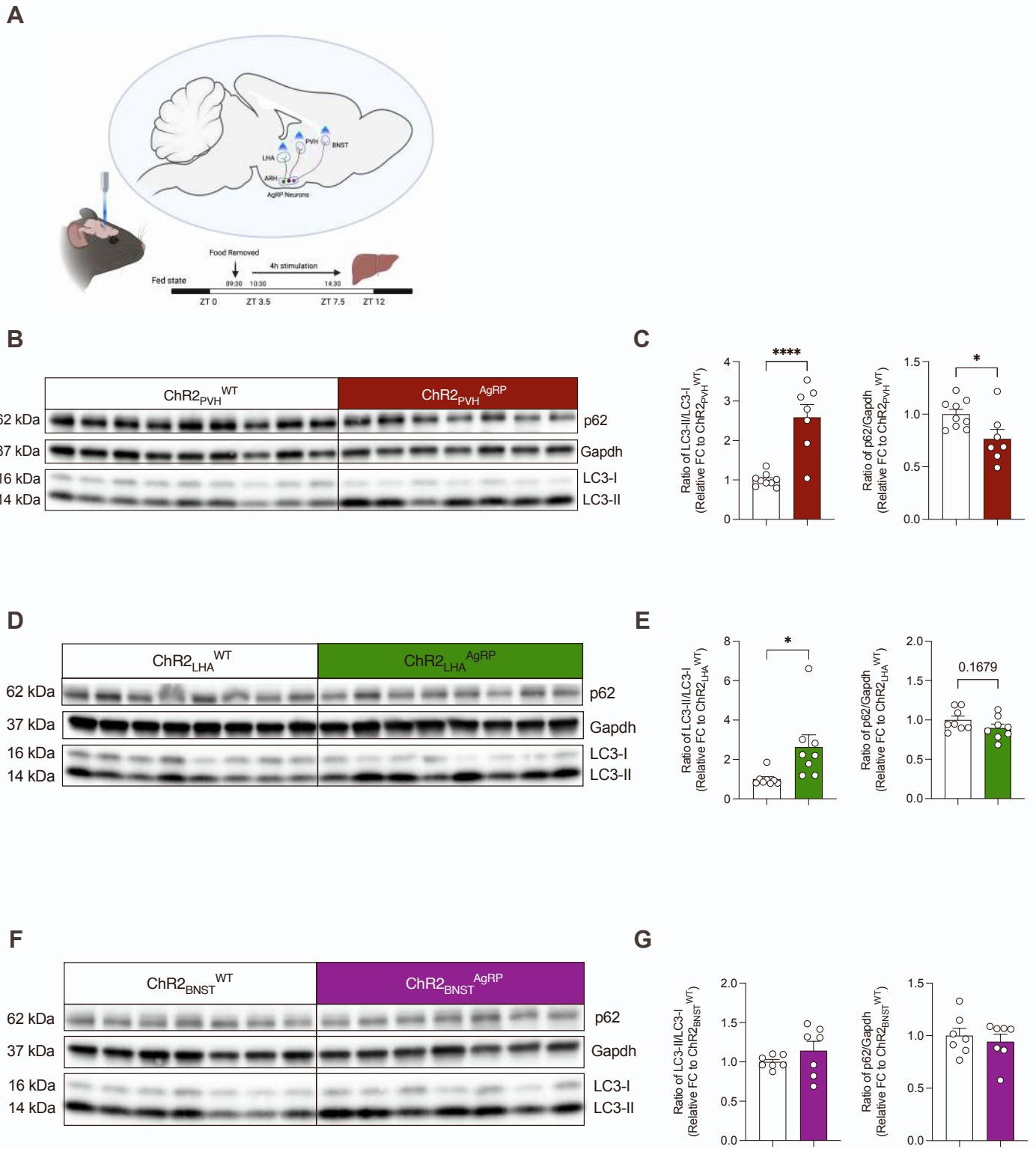
Supplemental Figure 8

A

B

C

D

E

F

G

Figure S8. AgRP→PVH and AgRP→LHA but not AgRP→BNST terminal stimulation evoke autophagy in the liver, related to Figure 3.

(A) Workflow and experimental design for optogenetic activation of AgRP neuron projection terminals.

(B) Representative Western blots of fed ChR2^{WT} and ChR2^{AgRP} mice after 4 h of AgRP→PVH projection stimulation.

(C) Densitometric analysis of the ratio of LC3-II/LC3-I (LC3) and p62/Gapdh as autophagic marker proteins in liver homogenates from mice in (B) (n = 7-9 animals/group).

(D) Representative Western blots of fed ChR2^{WT} and ChR2^{AgRP} mice after 4 h of AgRP→LHA projection stimulation.

(E) Densitometric analysis of the ratio of LC3-II/LC3-I (LC3) and p62/Gapdh as autophagic marker proteins in liver homogenates from mice in (D) (n = 8 animals/group).

(F) Representative Western blots of fed ChR2^{WT} and ChR2^{AgRP} mice after 4 h of AgRP→BNST projection stimulation.

(G) Densitometric analysis of the ratio of LC3-II/LC3-I (LC3) and p62/Gapdh as autophagic marker proteins in liver homogenates from mice in (F) (n = 7 animals/group).

Data are represented as mean ± SEM. Statistical analyses were performed by unpaired two-tailed Student's t test. *$p \leq 0.05$; **$p \leq 0.01$; ***$p \leq 0.001$, ****$p \leq 0.0001$. (See also Suppl. Figures S7, S9).
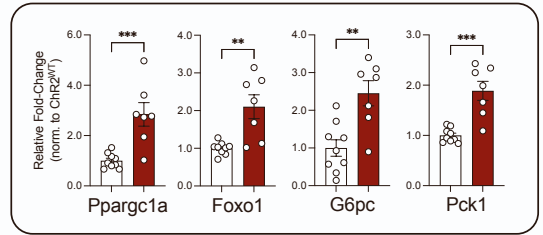
Supplemental Figure 9

A

Autophagy
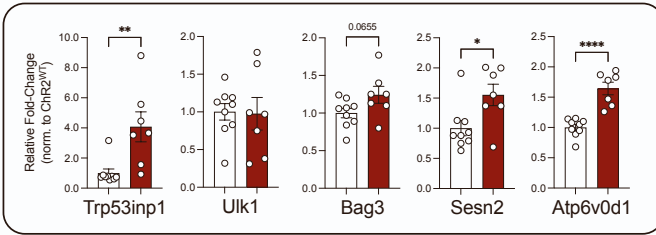
Glucose metabolism

Lipid Metabolism

B

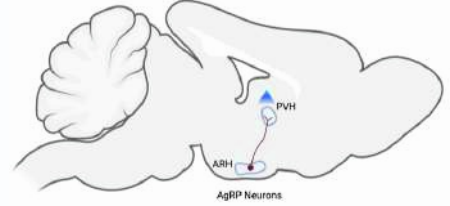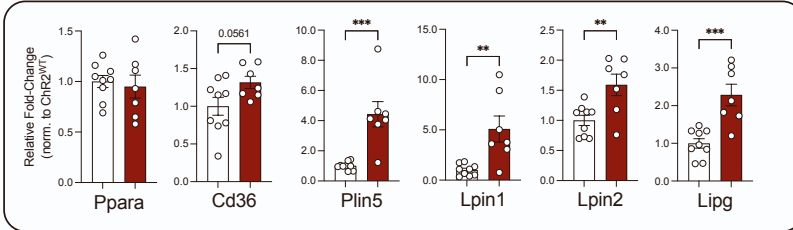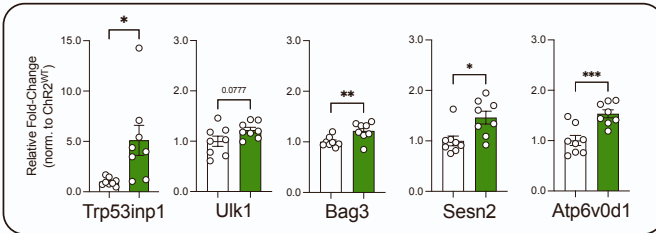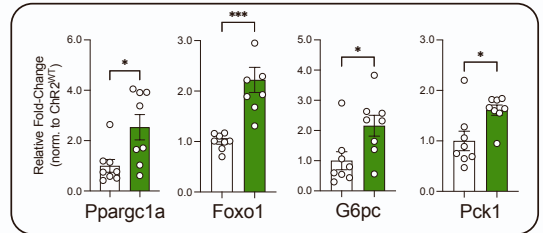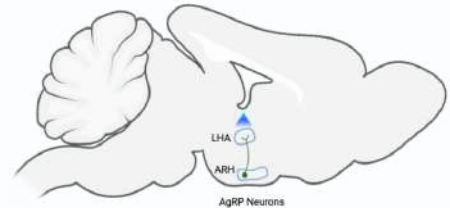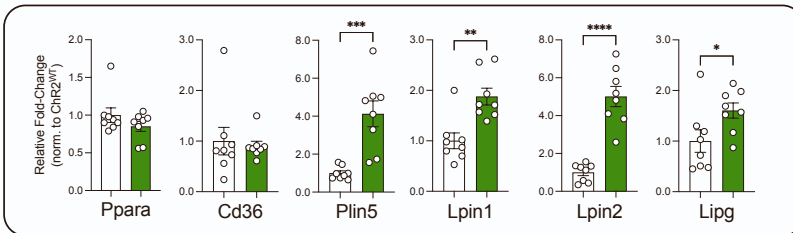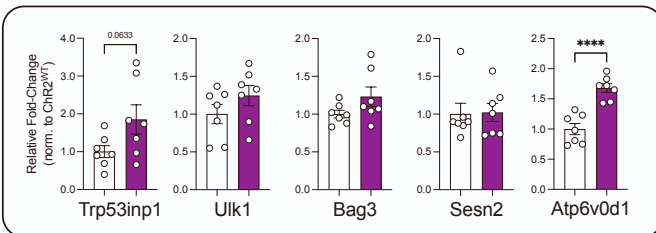### Autophagy

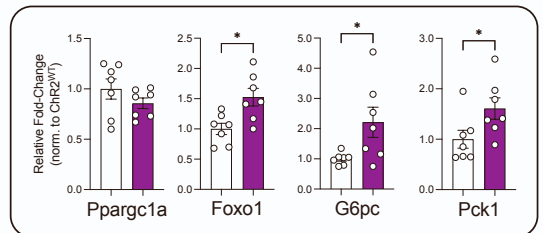### Glucose metabolism

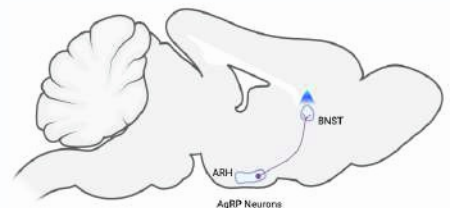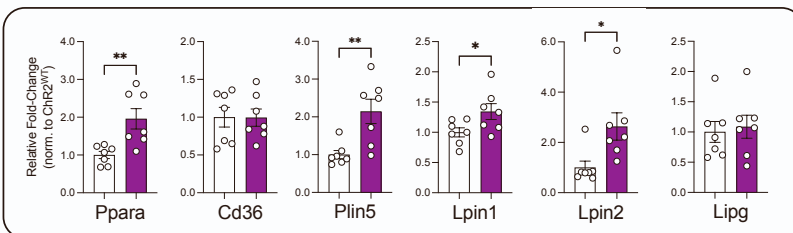

Lipid Metabolism

C

Autophagy

Glucose metabolism

Lipid Metabolism

Figure S9. AgRP terminal stimulation regulates hepatic gene expression, related to Figure 3.

(A)   Quantitative real-time PCR analyses of genes related to autophagy, glucose, lipid metabolism and fatty acid oxidation; data are normalized to ChR2$_{PVH}$^{WT} littermates and represented as scatter dot plots with individual values relative to *Tbp* expression (n = 7-9 animals/group).

(B)   Quantitative real-time PCR analyses of genes related to autophagy, glucose, lipid metabolism and fatty acid oxidation; data are normalized to ChR2$_{LHA}$^{WT} littermates and represented as scatter dot plots with individual values relative to *Tbp* expression (n = 8 animals/group).

(C)   Quantitative real-time PCR analyses of genes related to autophagy, glucose, lipid metabolism and fatty acid oxidation; data are normalized to ChR2$_{BNST}$^{WT} littermates and represented as scatter dot plots with individual values relative to *Tbp* expression (n = 7 animals/group).
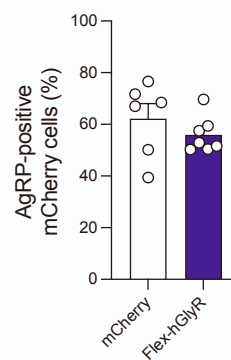
Data are represented as mean ± SEM. Statistical analyses were performed by unpaired two-tailed Student's t test. *$p \leq 0.05$; **$p \leq 0.01$; ***$p \leq 0.001$, ****$p \leq 0.0001$. (See also Suppl. Figure S6).

Supplemental Figure 10

A

B

C

Cohort 2 (Remaining samples for quantification)
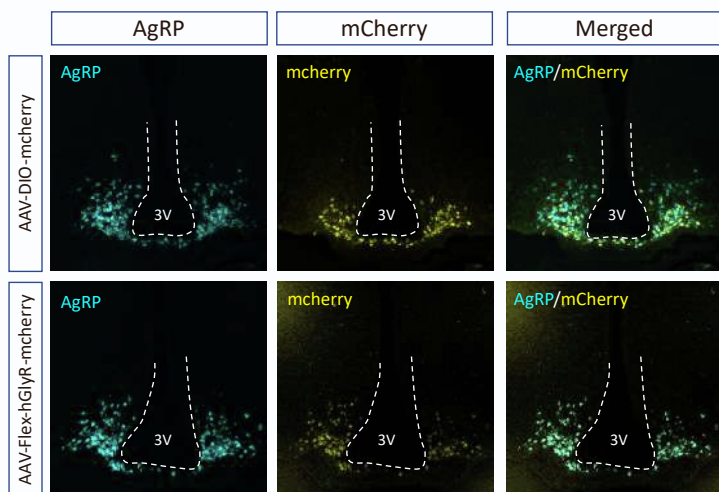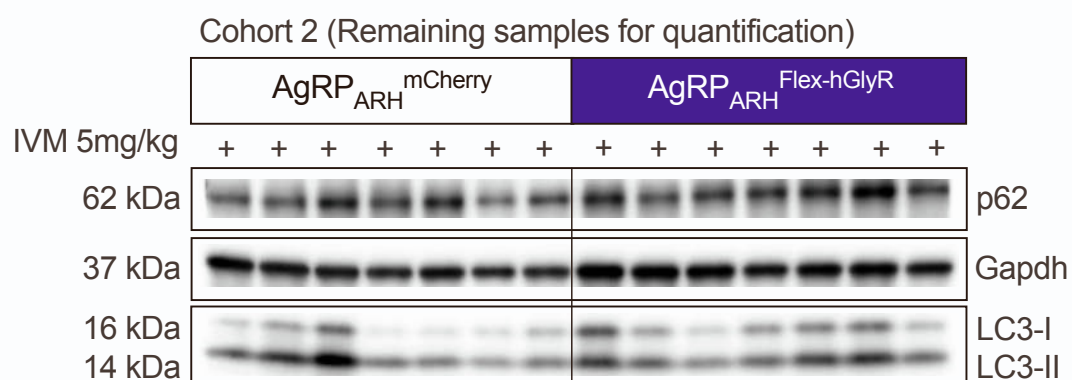
Figure S10. AgRP neuron activation is required for fasting-induced activation of hepatic autophagy, related to Figure 4.

(A) Representative micrographs showing *AgRP* (Cyan) and *mCherry* (Yellow) mRNA in the ARH, indicative of exclusive and successful bilateral expression of AAV-DIO-control and AAV-Flex-hGlyR.

(B) Percentage of mCherry-positive of AgRP cells as a measure for the efficiency of Cre-dependent expression of AAV-DIO-control and AAV-Flex-hGlyR in AgRP-IRES-Cre mice (n = 6-7 animals/group).

(C) Western blot showing the remaining replicates for the quantification of hepatic autophagic markers (LC3 and p62) after chemogenetic inhibition of AgRP during a short-term fast in the night cycle, related to Figure 5E.
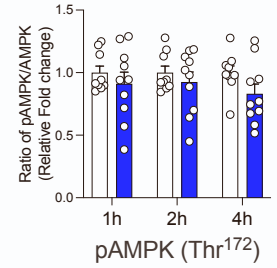
Data are represented as mean ± SEM.

Supplemental Figure 11

A

32 kDa — pS6 (Ser$^{235/236}$)
32 kDa — S6

Ratio of pS6/S6 (Relative Fold change)

pS6 (Ser$^{235/236}$)

B

62 kDa — pAMPK (Thr^{172})
62 kDa — AMPK
37 kDa — Gapdh

Ratio of pAMPK/AMPK (Relative Fold change)

pAMPK (Thr^{172})

C

60 kDa — pAKT (Ser^{473})
60 kDa — AKT
37 kDa — Gapdh

Ratio of pAKT/AKT (Relative Fold change)

pAKT (Ser^{473})

D

65 kDa — pAtg14 (Ser^{29})
65 kDa — Atg14
37 kDa — Gapdh

Ratio of pAtg14/Atg14 (Relative Fold change)

pAtg14 (ser^{29})

E

65 - 70 kDa — TFEB
37 kDa — Gapdh

Ratio of Tfeb/Gapdh (Relative Fold change)

TFEB

Figure S11. Time-dependent effects on AMPK, S6, AKT and TFEB signaling upon AgRP neuron activation, related to Figure 5.

(A)   Representative Western blot and densitometric analysis for pS6 (Ser$^{235/236}$) in liver homogenates from 1 h, 2 h and 4 h optogenetically stimulated ChR2^{WT} and ChR2^{AgRP} mice, (n = 9-10 animals/group/timepoint).

(B)   Representative Western blot and densitometric analysis for pAMPK (Thr^{172}) (n = 9-10 animals/group/timepoint). Gapdh was used as loading control.

(C)   Representative Western blot and densitometric analysis for pAKT (Ser^{473}) (n = 9-10 animals/ group/timepoint). Gapdh was used as loading control.

(D)   Representative Western blot and densitometric analysis for pAtg14 (Ser^{29}) (n = 9-10 animals/ group/timepoint). Gapdh was used as loading control.

(E)   Representative Western blot and densitometric analysis for TFEB/Gapdh (n = 9-10 animals/ group/timepoint). Gapdh was used as loading control.
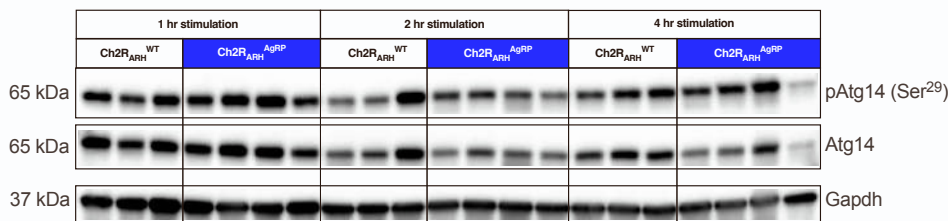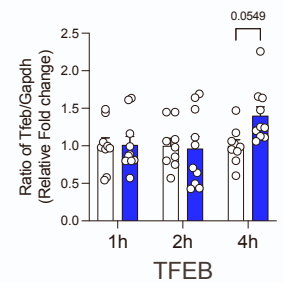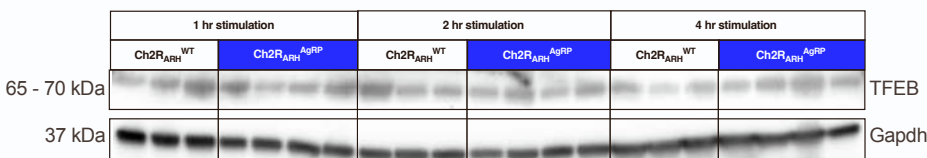
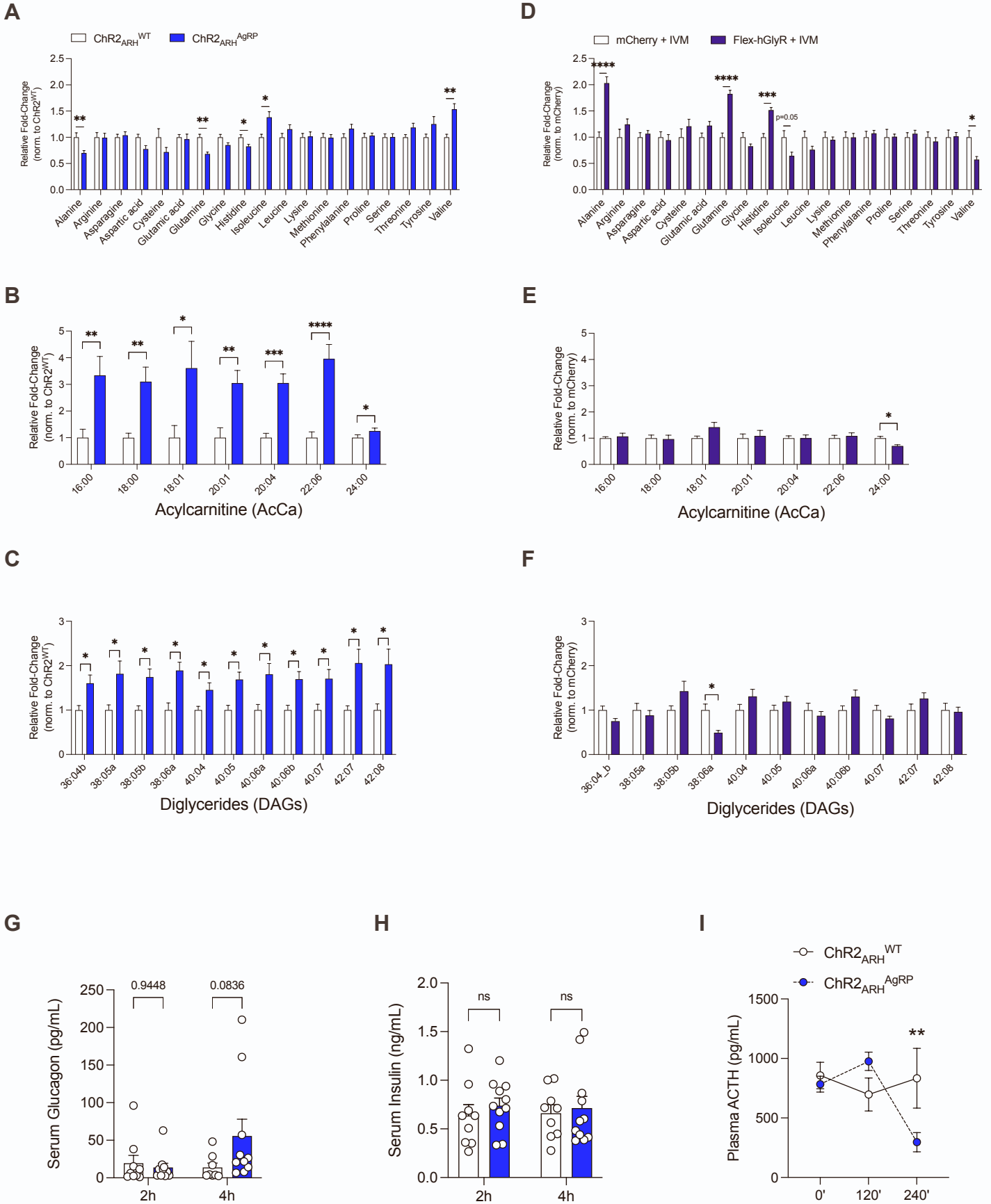Data are represented as mean ± SEM. Statistical analyses were performed by two-way ANOVA followed by Šídák post hoc test. ns = not significant, *$p \leq 0.05$; **$p \leq 0.01$; ***$p \leq 0.001$, ****$p \leq 0.0001$.
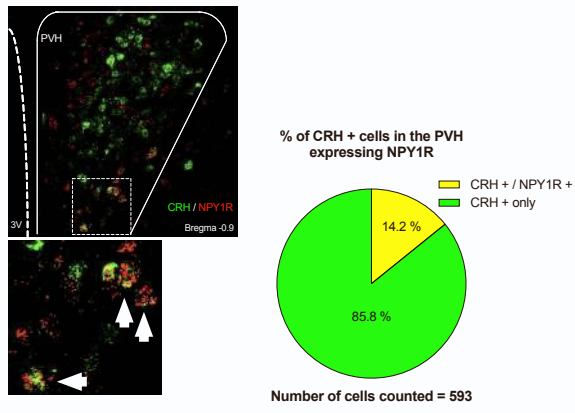
Supplemental Figure 12

Figure S12. AgRP neuron activation increases specific acylcarnitines and diglycerides species in the liver, however circulating glucagon and insulin levels remain unaltered, related to Figure 5 and 6.

(A)   Changes in specific amino acids in the liver after 4 h photostimulated ChR2^{WT} and ChR2^{AgRP} mice (n = 10-12 animals/group).

(B)   Altered acylcarnitines species in the liver following 4 h optogenetic activation of AgRP neuron (n = 9-14 animals/group).

(C)   Altered diglycerides species in the liver following 4 h optogenetic activation of AgRP neuron (n = 9-14 animals/group).

(D)   Changes in specific amino acids in the liver following a short-term 4 h fast and simultaneous chemogenetic inhibition of AgRP neuron (n = 13-14 animals/group).

(E)   Identical species of acylcarnitines in the liver which are significantly altered after optogenetic activation of AgRP neuron (n = 13-14 animals/group).

(F)   Identical species of diacylglycerides in the liver which are significantly altered after optogenetic activation of AgRP neuron (n = 13-14 animals/group).

(G)   Serum glucagon concentrations after 2 h and 4 h photostimulation of AgRP neuron (n = 8-10 animals/group/timepoint)

(H)   Serum insulin concentrations after 2 h and 4 h photostimulation of AgRP neuron (n = 9-11 animals/group/timepoint)

(I)   Longitudinal plasma ACTH measurements during 4 h photostimulation of AgRP neuron (n = 7-12 animals/group/timepoint)
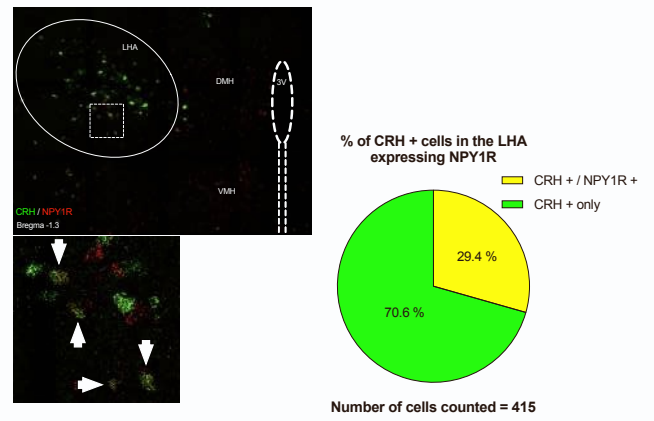
Data are represented as mean ± SEM. Statistical analyses were performed by multiple t-tests corrected with two-stage Benjamini, Krieger & Yekutieli FDR of 5% (for A-F) and two-way ANOVA followed by Šídák's post hoc test (for G, H; without RM and I; RM for timepoint stimulation) *p ≤ 0.05; **p ≤ 0.01; ***p ≤ 0.001, ****p ≤ 0.0001.

Supplemental Figure 13

A

% of CRH + cells in the PVH expressing NPY1R

- CRH + / NPY1R +
- CRH + only

14.2 %
85.8 %

Number of cells counted = 593

B

% of CRH + cells in the LHA expressing NPY1R

- CRH + / NPY1R +
- CRH + only

29.4 %
70.6 %

Number of cells counted = 415

C

PVH

% of cells in the PVH expressing NPY1R

7.2 %
92.8 %

Number of cells counted = 5428

- NPY1R + cells
- NPY1R - cells

% of NPY1R + cells surrounding PVH expressing SLC32A1

35.1 %
64.9 %

Number of cells counted = 148

- NPY1R + / SLC32A1 +
- NPY1R + only

% of NPY1R + cells in the PVH expressing SLC32A1 or SLC17A6

7.9 %
92.1 %

Number of cells counted = 391

- NPY1R + / SLC32A1 +
- NPY1R + / SLC17A6 +

D

E

NPY1R$_{PVH}$$^{AAV-hM4Di}$ (Saline)

18.7 %
81.3 %

Number of cells counted = 448

NPY1R$_{PVH}$$^{AAV-hM4Di}$ (CNO)

35.4 %
64.6 %

Number of cells counted = 580

- Non-activated CRH
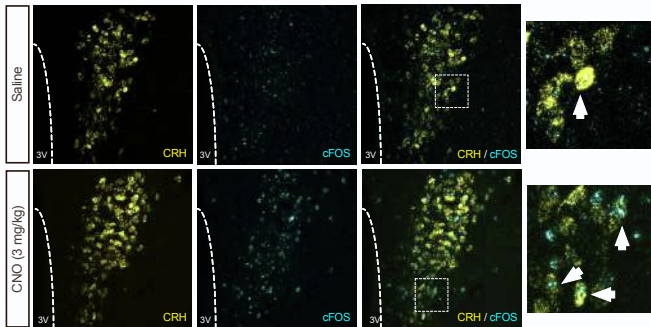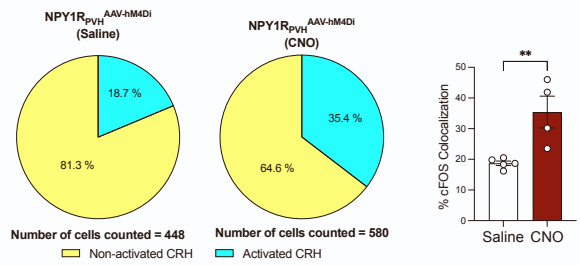- Activated CRH
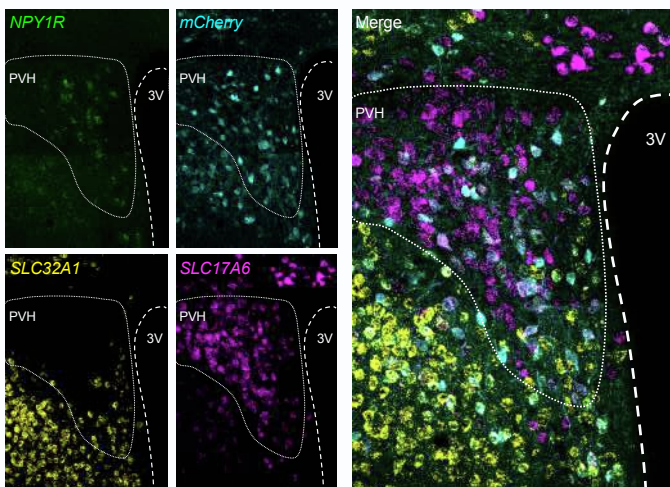

% cFOS Colocalization

**

Saline CNO

F

Figure S13. Chemogenetic PVH^{NPY1R} inhibition activates PVH^{CRH} neurons, related to Figure 3 and 6.

(A)   Representative confocal images showing *CRH* (Green) and *NPY1R* (Red) mRNA expression in the PVH of C57Bl/6N mice using *in situ* hybridization. Bottom panel depicts co-localization of CRH and NPY1R-expressing cells (Yellow) as indicated by white arrows. (Right) Percentage of NPY1R positive CRH cells in the PVH. Result indicates CRH+ *NPY1R*+ cells over total CRH+ cells counted.

(B)   Representative confocal images showing *CRH* (Green) and *NPY1R* (Red) mRNA expression in the LHA of C57Bl/6N mice using *in situ* hybridization. Bottom panel depicts co-localization of CRH and NPY1R-expressing cells (Yellow) as indicated by white arrows. (Right) Percentage of NPY1R positive CRH cells in the LHA. Result indicates CRH+ *NPY1R*+ cells over total CRH+ cells counted.

(C)   Representative confocal images showing *NPY1R* (Yellow) *SLC17A6* (Red) and *SLC32A1* (Cyan) mRNA expression in and surrounding the PVH of C57Bl/6N mice using *in situ* hybridization. Co-localization of *SLC17A6* (VGLUT2) or *SLC32A1* (VGAT) *positive* NPY1R-expressing cells are indicated by white arrows. (Right) Quantification expressed in percentage of NPY1R cells expressing *SLC17A6* or *SLC32A1* over total number of NPY1R+ cells counted in and surrounding the PVH.

(D)   Representative confocal images showing *CRH* (Yellow) and *cFos* (Cyan) mRNA expression in the PVH of saline or CNO-injected mice respectively. Right panel depicts activated CRH neuron indicated by white arrows.

(E)   Quantification of *cFos* positive CRH cells in the PVH using mRNA *in situ* hybridization. (Left) Results presented indicate the percentage of *Fos* positive cells over total CRH cells counted in (C). (Right) Statistical analysis of *Fos* positive CRH cells upon CNO-mediated inhibition of PVH^{NPY1R} neuron (n= 4-5 animals/treatment)

(F)   Representative confocal images showing *NPY1R* (Green), *mCherry* (Cyan), *SLC32A1* (Yellow) or *SLC17A6* (Magenta) mRNA expression in and surrounding the PVH of NPY1R-Cre mice injected with AAV-hM4Di-mCherry using *in situ* hybridization.

Data are represented as mean ± SEM. Statistical analyses were performed by unpaired two-tailed Student's t test (for E). **p ≤ 0.01.
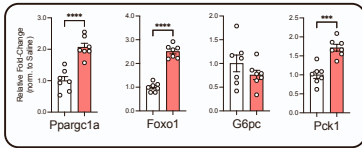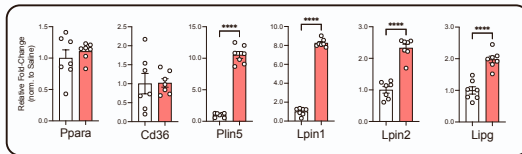
Supplemental Figure 14
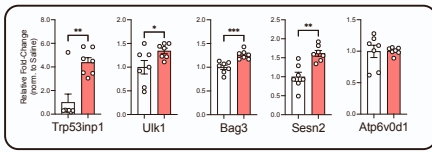
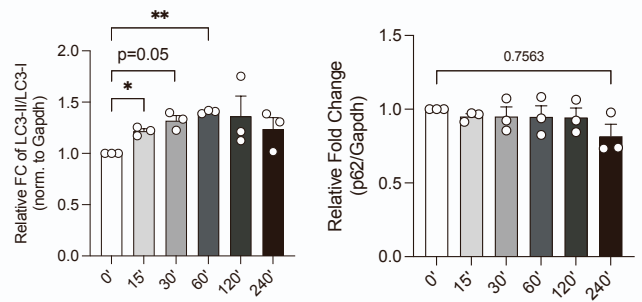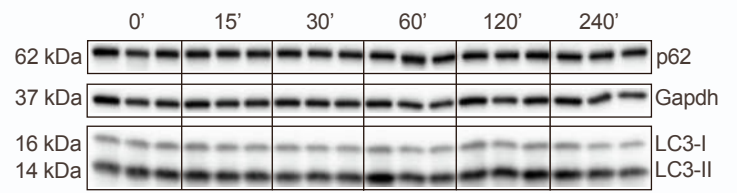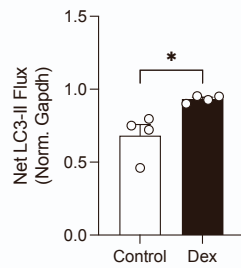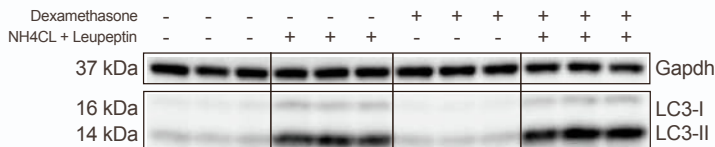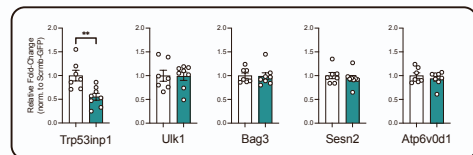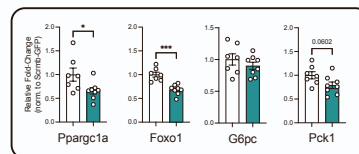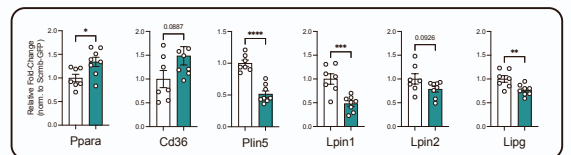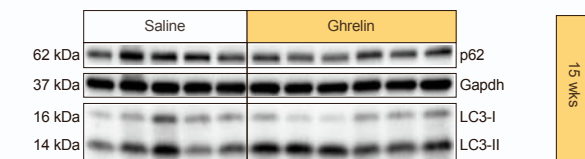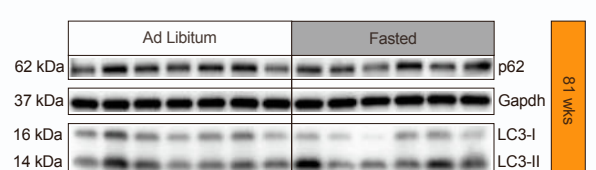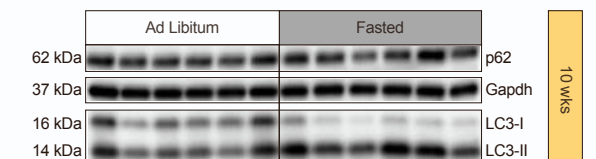**Figure S14. Aging impairs fasting and Ghrelin-induced liver autophagy and AgRP neuron mediates liver autophagy through glucocorticoid receptor expressed in the liver, related to Figure 6 and 7.**

(A)   Quantitative real-time PCR analyses of hepatic genes related to autophagy, glucose and lipid metabolism after a single application of ip Dexamethasone; data are normalized to saline treated and represented as scatter dot plots with individual values relative to *Tbp* expression (n = 7 animals/ group).

(B)   Representative Western blot and densitometric analysis of autophagic marker proteins from Hepa1-6 cells treated with 5 μM of dexamethasone for different periods (n = 3 independent experiments). Gapdh was used as loading control.

(C)   Representative Western blot and densitometric analysis of LC3-II/Gapdh in the presence or absence of lysosomal inhibitor from Hepa1-6 cells treated with 5 μM of dexamethasone for 4 h (n = 4 independent experiments).

(D)   Quantitative real-time PCR analyses of hepatic genes related to autophagy, glucose and lipid metabolism after 4 h of optically stimulating AgRP neuron with and without liver-specific knockdown of Nr3c1; data are normalized to Scrmb-injected mice and represented as scatter dot plots with individual values relative to *Tbp* expression (n = 7-8 animals/group).

(E)   Western blots of hepatic expression of autophagic markers (LC3 and p62) for individual 15 wks sand 78 wks old C57Bl6 mice after icv injection of saline or ghrelin. Gapdh was used as loading control.

(F)   Western blots of hepatic expression of autophagic markers (LC3 and p62) for individual 10 wks and 81 wks old C57Bl6 mice after ad libitum fed (AD) or fasted (F) for 4 h into the dark cycle respectively. Gapdh was used as loading control.

Data are represented as mean ± SEM. Statistical analyses were performed by one-way ANOVA followed by Dunnett's post hoc test (for B) or unpaired two-tailed Student's t test (for A, C and D). *p ≤ 0.05; **p ≤ 0.01; ***p ≤ 0.001, ****p ≤ 0.0001.